Gas-Solids Flow Structures in a Novel Circulating-Turbulent Fluidized Bed

Haiyan Zhu and Jesse Zhu
Dept. of Chemical and Biochemical Engineering, University of Western Ontario, London, ON N6A 5B9, Canada

DOI 10.1002/aic.11432
Published online March 31, 2008 in Wiley InterScience (www.interscience.wiley.com).

In this article a novel circulating-turbulent fluidized bed (C-TFB) featured by high solids holdup and high gross solids circulation has been introduced and tested. The purpose of the new design was to integrate conventional circulating and turbulent fluidized beds into a unique high-density fluidization system for more efficient gas-solid contact and significantly reduced solids backmixing. The hydrodynamic characteristics of the C-TFB were analyzed in terms of differential pressure, solids concentration, particle velocity, and local solids flux distributions. An axial homogeneous flow structure was easily obtained with cross-sectional average solids volume concentrations higher than 0.25 throughout the entire C-TFB. At all measuring positions there was no net downflow of solids and a good gas-solid mixing was observed. © 2008 American Institute of Chemical Engineers *AIChE J,* 54: 1213–1223, 2008
Keywords: circulating-turbulent fluidized bed, gas-solid fluidization, new design, high density, hydrodynamics, multi-phase flow, particle technology

Introduction

Conventional fluidized bed

With the advantages of good mass and heat transfer characteristics, gas-solids fluidized beds have been widely utilized in many industrial processes including combustion, gasification, catalytic cracking, calcinations, etc.[1,2] The performance of these multiphase fluidized bed reactors greatly depends on their hydrodynamic properties. From the experimental evidence available in the literature so far, gas-fluidized beds may operate in several different flow regimes: particulate fluidization, bubbling (slugging) fluidization, turbulent fluidization, fast fluidization, and pneumatic transport. While each of these flow regimes has encountered in industrial practice, the turbulent fluidization regime (turbulent fluidized beds) and fast fluidization [circulating fluidized beds (CFB)] cover the operations of almost all the key commercial applications[3] because of their own favorable fluidization characteristics.

Correspondence concerning this article should be addressed to J. Zhu at jzhu@uwo.ca.

Industrial applications of CFBs started in the 1950s, and rapidly expanded since late 1970s. Usually CFBs operate in the regime of fast fluidization with higher flow rate of gas and solids, leading to a higher production capacity and reduced axial gas back mixing. In addition, the independent control of gas and solids retention times provides the reactor more flexibility in operation. Previous experiments have clearly demonstrated that CFB is hydrodynamically characterized by an extremely nonuniform flow structure, with a dense bottom region and dilute upper region in the axial direction[4–6] and a "core-annulus" flow structure in the radial direction.[7–9] This nonuniform flow structure and relatively dilute solids concentration (usually less than 10%) result in many disadvantages, such as the serious gas by-passing through the core dilute region and extensive backmixing of solids in the wall region, consequently resulting in lower gross gas-solids contact efficiency and poor selectivity of chemical reactions.[10] Also there is a reduction in heat transfer coefficients between heat transfer surfaces and suspension and somewhat greater temperature gradients than in dense beds.[11,12] These limitations greatly affect the application of conventional CFBs' to processes with slow reaction rates or requiring high heat transfer rates. Furthermore, due to the

study by Dry et al.[10] the gas-solids contact appeared to reach its peak at superficial gas velocity (U_g) around 2 m/s for a solids flow rate (G_s) exceeding 100 kg/m^2 s, and then decreased as the gas velocity was further increased. At U_g of 8 m/s, the contact efficiencies appeared to be significantly less than 100%, even at G_s approaching 200 kg/m^2 s. These results suggested that, despite many advantages like the high throughput per unit reactor volume and good gas-solids flow rate control, the overall gas-solids contacting efficiency and the state of axial and radial gas mixing in conventional CFBs was not optimal.

Apart from the CFB reactors, turbulent fluidized beds (TFBs) have also been widely used in various industrial processes because of the vigorous gas-solids contacting, favorable bed-to-surface heat transfer, and high solids concentration (typically 25–35% by volume).[13] The surface-to-bed convective heat transfer coefficients tend to reach a maximum in the turbulent fluidization and the interphase mass exchange is also rapid. The high solids concentration combined with the efficient gas-solid contact and the temperature uniformity in TFBs is a very attractive operating mode for industrial applications. However, compared with CFBs, more serious backmixing of both gas and solids phases occurs in TFBs.

High density/high flux circulating fluidized bed risers

The concept of high-density CFB operation was first proposed by Bi and Zhu[14] to distinguish the high-flux and high-density operating conditions encountered in FCC risers from those low flux and low-density operations corresponding to the CFB combustors. In 1995, Zhu and Bi[15] further defined the high-density operation with $G_s > 200$ kg/m^2 s and $\varepsilon_s >$ 3–5% in the developed section of the riser. Among the studies exploring high-density/high-flux fluidized beds, the most comprehensive research work has been carried out at the University of British Columbia[3,6,16–20] and the University of Western Ontario[21–23] with Group A particles (FCC). In UBC's work, it was found that under high fluxes and suspension densities (U_g = 4–8 m/s, G_s = 200–425 kg/m^2 s) there was no net downflow of particles at the wall and cross sectional averaged solids volumetric concentration was about 0.1–0.25 with little axial variation. In 1999, Grace et al.[18] proposed a new flow regime named "dense suspension upflow" (DSU) to represent the flow dynamics inside the high-density riser and claimed that this flow regime "clearly requires both high superficial gas velocities (at least several m/s) and high solids fluxes (at least 200 kg/m^2/s)". UWO's studies were conducted in a relatively long riser (10 m in height compared to 6.1 m riser used in UBC). Their results showed that under high-flux operations (U_g = 5.5–10 m/s, G_s = 300–550 kg/m^2 s), the axial solids concentration profile was not flat and the cross-sectional solids concentration was clearly less than 0.1 in the upper portion of the riser with a dense bottom region ($\varepsilon_s \sim 0.2$). Radial solids concentration profiles at high G_s (>300 kg/m^2 s) were less uniform than that of lower G_s (<200 kg/m^2 s).

In both groups' studies, the solids volume concentrations were found to be lower than 0.06 in the central region ($r/R < 0.5$) and increased to 0.4–0.44 at the wall region. This strong radial solids concentration gradient may result in similar gas bypassing phenomenon as occurred in typical CFBs, that reduces the gas-solids contact intensity.

Concept of circulating-turbulent fluidized bed

Current research in fluidized bed reactors continues to explore means of improving reactor performance with better gas-solids contacting efficiency and higher conversion per unit volume. A natural development is to take the technology a step further with better hydrodynamic characteristics. In this article a novel circulating-turbulent fluidized bed (C-TFB) was proposed, where a special operating mode with low superficial gas velocity and high solids circulation rate was realized, resulting in a highly dense suspension and uniform flow structure. The C-TFB design and operation was developed especially to overcome a number of problems usually encountered in CFB risers and TFBs, while integrating the advantages of both, such as the high solids concentration, excellent gas-solids contact efficiency, as well as the suppression of axial mixing with high solids circulation rates.

High solids flow rates and uniform dense suspension will be very useful for applications requiring higher solid/gas feed ratios and uniform solids and gas residence time, slow reactions involving both gas and solids phases, and processes where the gas-solid contacting efficiency is crucial.

It is thought that the C-TFB can create the following advantages over the conventional fluidized beds:

(1) Recycling particles, while maintaining a high solids concentration and gas-solid reaction intensity;

(2) High particle handling capacity with low gas by-passing;

(3) No net downflow of solids over the whole section;

(4) Axial homogenous flow structure and enforced homogeneity of suspension in radial direction.

Hydrodynamic characterization of the novel C-TFB has been carried out in a cold-flow set-up. Results of measurements of pressure drop, local solids concentration, particle velocity, and solids flux were presented in this article.

Experimental Setup

The conceptual C-TFB was shown schematically in Figure 1. The system consists of six parts: (1) a C-TFB column, with i.d. of 0.101 m and height between gas distributor (a perforated-plate with open area ratio 14%) and column top of 3.6 m; (2) a quick discharging section at the top of the C-TFB column with a diameter of 0.203 m and a total height of 6.4 m; (3) a downcomer (i.d. 0.305 m) with total solids inventory of about 420 kg, equivalent to a solids level of $\sim$6 m in the downcomer when all solids are stored there; (4) a solids circulation rate measurement device with two flapper valves in the upper section of the downcomer (see Pärssinen and Zhu's paper[21] for more details); (5) a recycle loop including a primary inner cyclone, secondary and tertiary standard cyclones, and a bag filter to capture the entrained particles and return them to the downcomer; (6) an inclined solids return pipe at the bottom with a solid circulation flow rate control device.

After passing the butterfly valve in the inclined pipe, the solids coming from the downcomer entered the C-TFB bottom at a height of 0.2 m above the gas distributor, and were accelerated by air at ambient conditions. Secondary air sup-

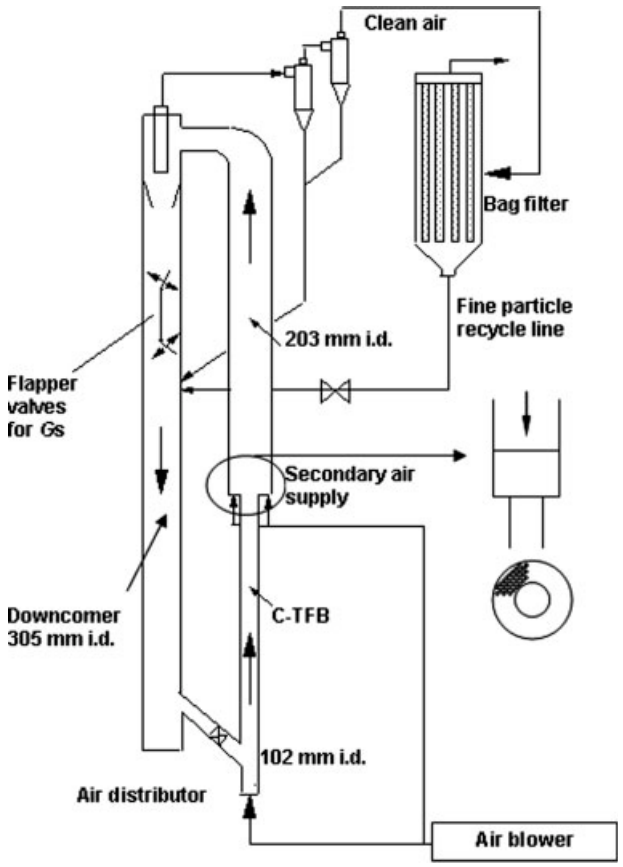

Figure 1. Schematic drawing of the C-TFB.

ply was distributed via an annular perforated plate with 12.6% free area at the bottom of the discharging column to lift the particles upwards and to entrain particle out of the column as quickly as possible, so that the pressure drop in the upper section was minimized. Therefore, this unique design enabled high solids circulation rates and high suspension density in the C-TFB with relatively low superficial gas velocity (1–3 m/s). The air flow rates were individually controllable in each of the columns, and such flexible operation was indeed a very important design aspect for a technology needed to operate over a wide range of gas to solids loading ratios. In the present study, the secondary air velocity was kept at 5 m/s.

The particles used in this study were FCC catalyst with a Sauter mean diameter of 65 μm and a particle density of 1780 kg/m^3. The relative humidity was kept between 50 and 60% to limit the electrostatic effects and the capillary forces to acceptable levels.[24] The particle size distribution was listed in Table 1.

Table 1. Size Distribution of the FCC Particles

Particle Size (μm)	Volume Fraction (%)
0–20	1.71
20–40	29.48
40–60	35.01
60–80	19.37
80–110	10.83
110–160	3.61

Experimental measurements included differential pressure and local solids concentration and particle velocity. Five pressure taps were installed over 0.7 m intervals along the C-TFB and connected with four differential pressure transducers (Omega PX162) to measure the axial profiles of the pressure gradient. To prevent particles from entering the measuring lines, the pressure taps were covered with fine screens. Signals of the differential pressure fluctuations were sampled with a frequency of 1000 Hz and the total acquisition time was 30 s.

Local solids concentration and velocity were measured using two optical fiber probes (Probe 1 and Probe 2, as shown in Figure 2) at four axial positions (0.8, 1.5, 2.2, and 3.0 m), and at eleven radial positions (r/R = 0.0, 0.16, 0.38, 0.5, 0.59, 0.67, 0.74, 0.81, 0.87, 0.92, and 0.98) at each axial level. The optical fiber probes were model PV-5, newly developed by the Institute of Process Engineering, Chinese Academy of Sciences, Beijing, China. The optical fiber probes were capable of simultaneously measuring instantaneous solids concentration and particle velocity. The probe diameter was 4 mm, containing two sub-probes with an active tip area of 1 $\times$ 1 mm for each, with a separation distance of 1.7 mm. Each sub-probe consisted of both light-emitting and receiving quartz fibers arranged in an alternating array, corresponding to emitting and receiving layers of fibers. The diameter of each fiber was 25 μm. To prevent particles from occupying the blind zone, a glass cover (0.2 mm) was placed over the probe tip. The received light reflected by the particles was converted by a photo-multiplier into voltage signals. The voltage signals were further amplified and fed into a PC. At each location the data were sampled at 50 kHz for 30 s. At least five repeat measurements were made. This combination of the sampling rate and sampling length ensured that the full spectra of hydrodynamic signals of interest were captured from the fluidized bed. Using a calibration equation the voltage data were converted to solids concentrations and the calibration process was described in detail by Zhang et al.[25]

Since the reflective optical fiber probe was an intrusive measurement technique, the impacts of the two probes on the overall flow structure were tested under four operating conditions, listed in Table 2, at axial position Z = 1.5 m and 10 radial position r/R = 0.16, 0.38, 0.5, 0.59, 0.67, 0.74, 0.81, 0.87, 0.92, and 0.98. First, for each operating conditions

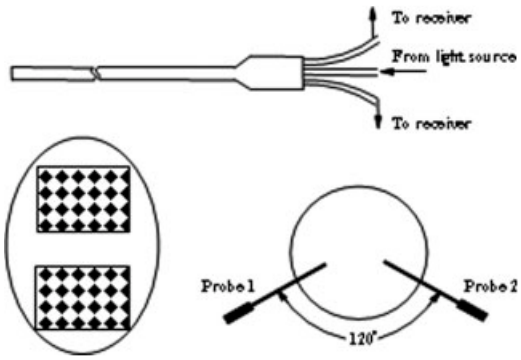

Figure 2. Schematic of the solids concentration-velocity fiber optic probe.

Table 2. Operating Conditions in C-TFB

G_s = 50 kg/m^2 s		G_s = 150 kg/m^2 s	
U_g = 1.0 m/s	U_g = 2.0 m/s	U_g = 1.0 m/s	U_g = 2.0 m/s

the solids concentration was measured five times with just probe no. 1 at 10 radial positions. The sampling frequency was 50 kHz and the duration of measurement 30 s. Solids concentration and standard deviation were calculated for each measurement. Then, the same measurement procedure was repeated with probe no. 1 after the probe no. 2 was inserted into the column with tip locating at the same radial position of probe no. 1. For all operating conditions and at all radial positions, a good agreement observed between the solids concentrations and standard deviations before and after the probe no. 2 was inserted with 0.02 maximum differences. Hence, it was assumed that the existing of the two probes has no significant interference on the over all flow structure.

In principle, when vertically moving particles passed the tips of two sub-probes, similar signals with difference of only a shift in time would be measured. Therefore, the vertical particle velocity could be calculated with cross-correlation method. In this study, an integration time T of 20.5 ms was set, and there were totally 1460 groups for each sampling. Elimination criteria were employed to systematically remove poorly correlated data (cross correlation coefficient less than 0.6, as used by Werther et al.[26]). It was impossible to directly confirm this method as an accurate method for measuring local particle velocity without using another method. However, when the net solids flux G_s^* calculated from Eq. 1 was integrated across the riser cross-section and compared with the overall solids circulation rate G_s measured by the flapper valves in the measuring tank, a reasonably accurate mass balance was established. This validated the accuracy of both particle velocity and solids volume concentration (V_p and ε_s, respectively) measured by the probes.

$$G_s^* = \frac{1}{\pi R^2}\int_0^R 2\pi r \overline{G}_{s,L}\, dr = 2\int_0^1 \overline{G}_{s,L}\frac{r}{R}d(r/R) \qquad (1)$$

$$\overline{G}_{s,L} = \rho_p \int_0^T V_p(t)\varepsilon_s(t)\, dt \qquad (2)$$

Here, $\overline{G}_{s,L}$ was the time-mean local solids flow rate, $V_p(t)$ was the instantaneous particle velocity and $\varepsilon_s(t)$ was instantaneous solids concentration measured with the probes. Figure 3 showed the comparison between G_s measured by the measuring tank and G_s^* calculated by Eq. 1. The error was less than 5%, demonstrating that the measured particle velocity and solids volume concentration were reliable.

In the present work the hydrodynamic studies were carried out first to establish the feasibility and then to characterize the behavior of the proposed system. The operating conditions were listed in Table 2. The effects of solids loading and superficial gas velocity on the performance of the proposed reactor were investigated. The results in comparison with normal CFBs and TFBs were also presented.

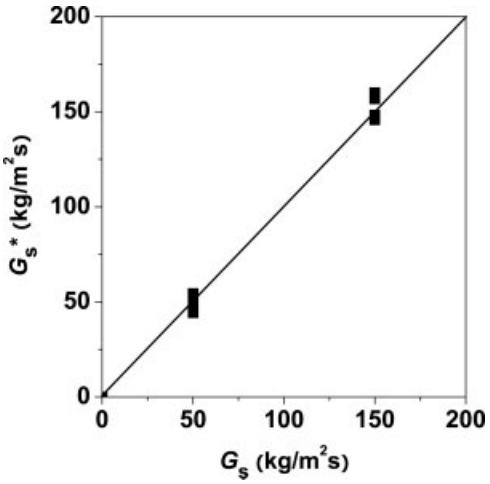

Figure 3. Measurements validation for solids concentration-velocity optical fiber probe.

Results and Discussion

Axial differential pressure profiles

Differential pressure profiles were used first to characterize the global hydrodynamic behavior in the C-TFB. Results under steady state operations were displayed in Figure 4 for different superficial gas velocities (U_g) and solids circulation

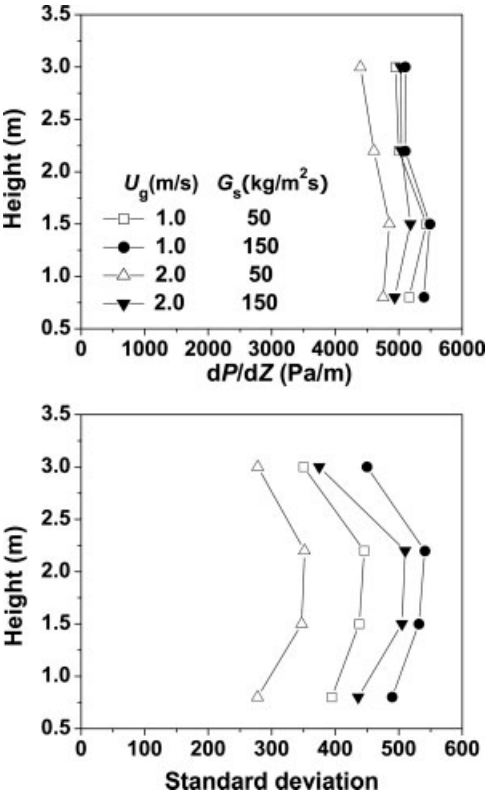

Figure 4. Differential pressure profiles along the C-TFB.

Table 3. Solid/Gas Loading Ratio

	G_s = 50 kg/m^2 s		G_s = 150 kg/m^2 s	
	U_g = 1.0 m/s	U_g = 2.0 m/s	U_g = 1.0 m/s	U_g = 2.0 m/s
Solid/gas ratio	41. 7	20.8	125	62.5

rates (G_s). The differential pressure profiles exhibited almost uniform distributions along the C-TFB under all four operating conditions. The differential pressures increased with increasing G_s and/or decreasing U_g, but the increase was limited as the bed condition was already fairly dense.

Gas-solid interfacial area per unit volume of suspension that directly affects gas-solid reaction is very much related to the solids distribution. Solids residence time distribution within the fluidized bed and heat transfer between the suspension and the wall are also dependent on the solids distribution. It has been found that particle convective heat transfer coefficient increases with the solids suspension density because of higher particle thermal conductivity.[27] In this C-TFB, apparent cross-sectional averaged solids concentration calculated from the differential pressure measurements ($\Delta P/\Delta Z = [\rho_s \varepsilon_s + \rho_g(1 - \varepsilon_s)]g$) ranged from 0.25 to 0.30. Such a high solids concentration condition should ensure excellent heat and mass transfer rates in the proposed new fluidized bed reactor for many chemical processes with moderate and slow reactions.

The corresponding standard deviation profiles were also included in Figure 4. Consistent with the differential pressure profiles, the standard deviation values also increased with increasing G_s and/or decreasing U_g, reflecting the increased flow fluctuations caused by particle–particle interactions. Under all operating conditions, the fluctuation increased with the height first, and reaches its maximum at the middle region of the C-TFB (Z = 1.5 and 2.2 m), and then decreases with height. The maximum standard deviation reflected the vigorous particle–particle interactions at the middle region.

Solid-to-gas loading ratio, $G_s/(\rho_g U_g)$, is the dimensionless solids circulation rate. Values under the four operating conditions as summarized in Table 3 showed that the solid/gas loading ratio could reach as high as 125 in the C-TFB, in comparison of 10–80 for most CFB operations with Group A particles.

Comparing these solid-to-gas loading ratios with the shapes of the differential pressure profiles, it could be noted that for solid-to-gas loading ratios larger than 40, the differential pressure became more uniform along the C-TFB, and only changed little with further increasing the loading rate. To examine further the flow characteristics, the axial and radial solids distribution profiles in the column were measured by the optic probes.

Axial solids distribution profiles

It was widely recognized that for a better understanding of the flow properties in multiphase systems, such as CFB, it was of prime importance to know the inner details of such flows. Especially, the knowledge of the local solids distribution in the fluidized beds was key to successful design and operation of these systems. In this study, the local solids distributions were investigated in both axial and radial directions for four operating conditions.

The cross-sectional averaged solids concentrations along the C-TFB, as integrated from the local solids concentration profiles, were summarized in Figure 5. It was found that a uniform and dense gas-solid suspension has been achieved along the whole column, with solids volumetric concentrations ranging from 0.23 to 0.29. In particular, for the high solid-to-gas loading ratio cases (>40, as shown in Table 2), the averaged solids concentration was higher than 0.25 throughout the entire C-TFB. This solids volume concentration was higher than that in the bottom dense region of typical CFBs (~0.2) and that in the "DSU" (0.15–0.25) as reported by Issangya et al.,[6] Grace et al.,[18] Pärssinen and Zhu,[21] Louge and Chang,[28] and Malcus et al.[29] This high-density uniform axial solids distribution in the C-TFB was a significant advantage over conventional CFB, which have a substantial variation in cross-sectional averaged solids concentration with a dense phase at the bottom and a relatively dilute region towards the top.[5,12] The axial uniform flow structure should lead to both uniform solid-gas contact efficiency and uniform suspension-to-wall heat transfer throughout bed height.

Radial solids distribution profiles

The influence of the operating conditions (U_g, G_s) on the radial solids distribution was investigated at the height of Z = 2.2 m. As shown in Figure 6, except the case U_g = 2 m/s and G_s = 50 kg/m^2 s, the time mean solids concentration increased monotonically with the radial position, from 0.1 at the center to 0.45 at the wall, and such an increase followed the same trend within the tested range of operating conditions. Furthermore, changes in operating conditions have no significant influence on the radial solids concentration profiles. This insensitivity to the operating conditions suggested that the two-phase suspension density reached a saturation state in the C-TFB.

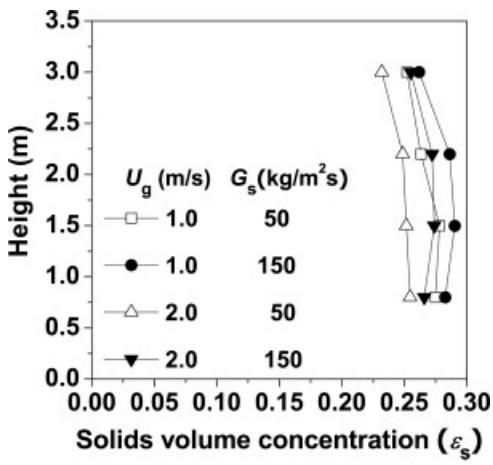

Figure 5. Cross-sectional averaged solids concentration.

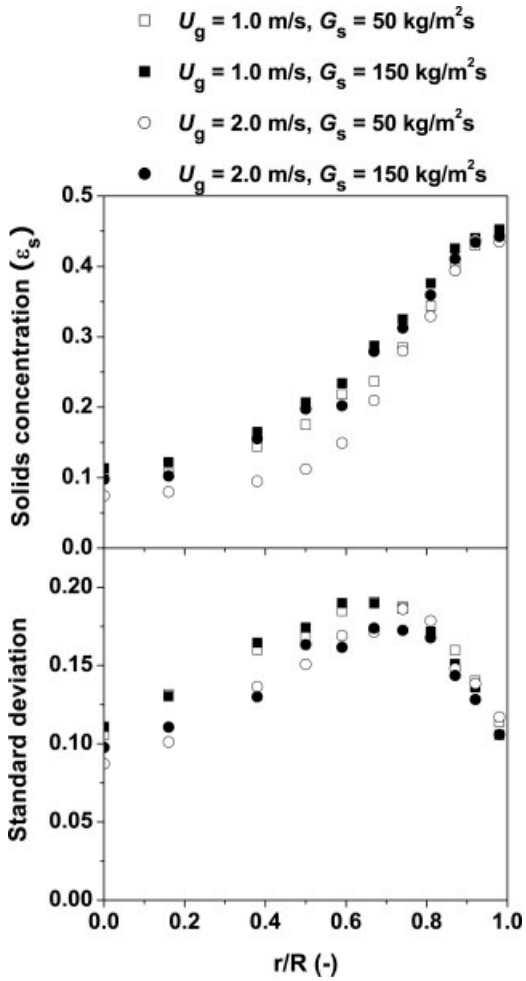

Figure 6. Effects of operating conditions on radial solids distribution Z = 2.2 m.

Figure 6 also plotted the corresponding standard deviations for the radial profiles. First, the fluctuation of solids concentration increased gradually to a peak at r/R = 0.6–0.7, and then underwent a sharp decrease towards the wall. The maxima in the solids concentration fluctuations indicated a vigorous gas-solids interaction at the corresponding radial position, which always occurred at the middle region of the column under all operating conditions. Such a phenomenon that the standard deviation peaked at middle radial position was also reported by Issangya et al.[17] and Grace et al.[18] in their high density CFB. They claimed this phenomenon as a special characteristic for high density CFB which were operated under relatively high superficial gas velocity, but it was clearly shown in C-TFB as well.

The flow development along the C-TFB was shown in Figure 7 at U_g = 1.0 m/s and G_s = 150 kg/m^2 s. The radial profiles of solids concentration from different axial positions were quite similar, with height increasing from 0.8 to 3.0 m. The solids concentration just decreased slightly in the center (from 0.16 to 0.09) but changes little at the wall. This result confirmed that the flow structure in the bed was axially homogeneous, as reflected in the differential pressure profiles (Figure 4). The insensitivity of solids concentration to the height suggested a fully developed dense solids flow over the entire bed. The

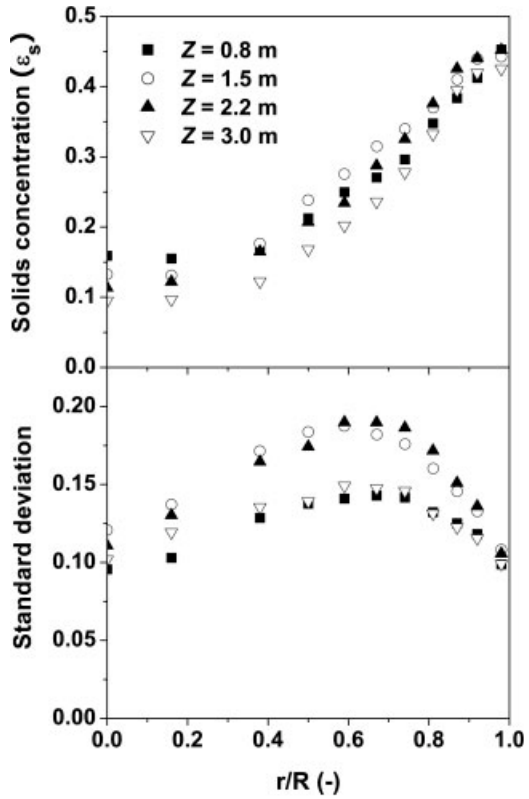

Figure 7. Radial profiles of solids distribution along C-TFB U_g = 1.0 m/s, G_s = 150 kg/m^2 s.

included standard deviation profiles at different heights showed that the magnitude of solids concentration fluctuations depended strongly on the radial position as well as on the axial position. The strongest fluctuations also appeared at the middle heights (Z = 1.5 and 2.2 m), which was in consistent with the differential pressure results shown in Figure 4.

Tangential symmetry of the solids flow inside C-TFB

Figure 8 presented the measurements from two different radial directions with an angle of 120° apart (as shown in

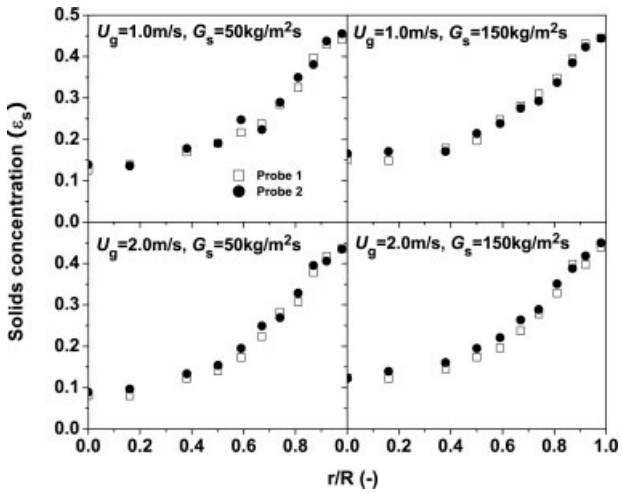

Figure 8. Radial symmetric flow structure at Z = 0.8 m.

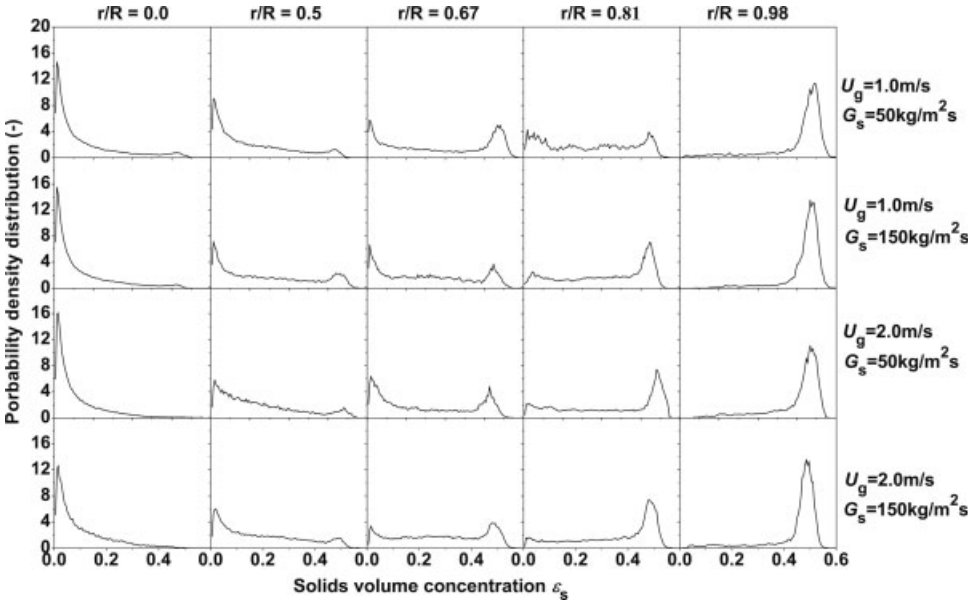

Figure 9. Probability density distribution in C-TFB at Z = 2.2 m.

Figure 2) at the same axial position Z = 0.8 m. The results showed that under all four operating conditions, there was little difference between the measurements obtained from the two directions. As such, the time-averaged local solids concentration exhibited a tangential symmetric distribution in the C-TFB, even at the low axial position, where the flow structure was prone to be affected by the gas distributor or solids inlet.

Probability density distributions

Instantaneous solids concentration has a considerable effect on the apparent reaction and heat/mass transfer properties in the fluidized beds.[30,31] To further explore the links between the fluctuations of solids concentrations and the interaction between the gas-solids phases, probability density distribution (PDD) analyses were carried out at Z = 2.2 m and five different radial positions. Typical PDD curves of local solids concentration signals were illustrated in Figure 9.

In general, three types of PDD curves were observed depending on the different radial positions. First, at the axis (r/R = 0.0), the probability distribution plot showed a single low concentration peak ($\varepsilon_s \sim 0.02$) with a long tail at right hand, indicating that a large amount of particles are in dilute phase (represented by $\varepsilon_s \sim 0.02$). Second, in the middle region, two-peak continuous solids concentration distribution with low probability density was observed and the distinction between the dense (represented by $\varepsilon_s \sim 0.5$) and dilute phases was diffuse or even lost completely. This broad distribution resulted in a better gas-solids contacting quality and further reduces gas by-passing, which occurred in the core region of conventional CFB risers as reflected by the narrow sharp peak distribution.[32] Third, moving outwards towards the wall, the low solids concentration peak disappeared and there was only a high-density peak with a long tail towards the left. For all three radial regions, there existed wide distributions of local solids concentration. This excellent mixing between the solids and gas phases represented by the broad distribution of PDD at almost all radial positions was a great advantage of C-TFB.

Particle velocity measurements

Particle velocities in fluidized beds were also of great interest in understanding local flow dynamics, as the particle velocity was directly related to the particle residence time in fluidized beds. From the optical fiber probe system, the velocities of both upflowing and downflowing particles, $V_{p,up}$ and $V_{p,down}$ respectively were obtained with the cross-correlation method.

Figure 10 showed the effects of operating conditions on the radial distributions of particle velocities at Z = 2.2 m.

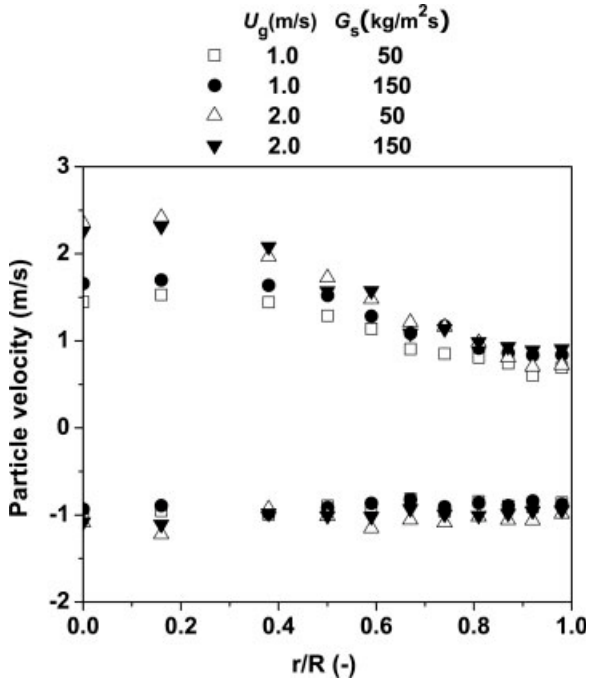

Figure 10. Effects of operating conditions on particle velocity at Z = 2.2 m.

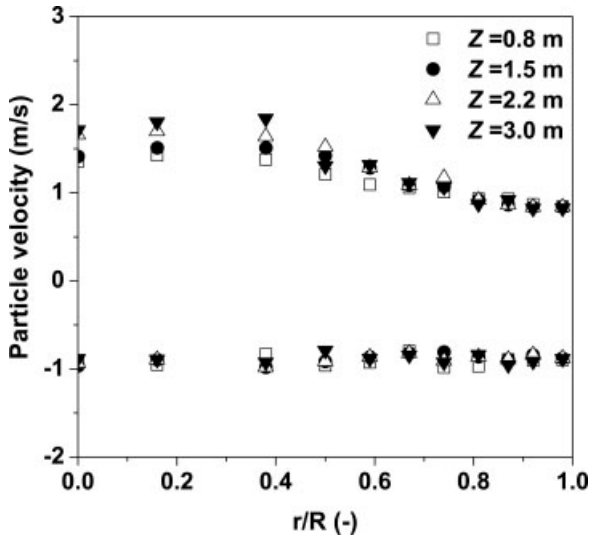

Figure 11. Axial positions effects on particle velocity distribution U_g = 1.0 m/s, G_s = 150 kg/m^2 s.

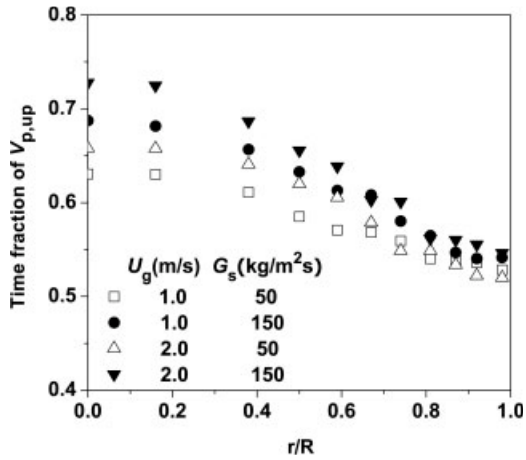

Figure 12. Time fraction of upflowing particle velocity at Z = 2.2 m.

Overall, it can be found that particles moved up and down dynamically at all measuring points. Increasing U_g led to an increase in the $V_{p,up}$ at all radial positions, with higher degree of increase in the center region. Compared with U_g, G_s has less effect on $V_{p,up}$. Results also showed that the $V_{p,down}$ remains relatively constant at about -1 m/s regardless of the radial position and operating condition.

To investigate the particle velocity distribution along the C-TFB, velocity measurements from different axial levels at U_g = 1.0 m/s and G_s = 150 kg/m^2 s were carried out. As shown in Figure 11, axial position has no significant effect on the particle velocity, especially in the wall region ($r/R >$ 0.6). Such a strong independence of particle velocity on the height could only be understood by considering that the gas-solids suspension reached some kind of "an equilibrium state," or "a force balance" in the macro-scope, so that there was no obvious solids acceleration along the C-TFB. Furthermore, the enhanced collision and interaction between the particles in the high-density flow conditions greatly unified the axial particle velocity distribution. These results showed a strong connection between the particle velocities and the status of overall solids flow structure in this extremely high-density gas-solids suspension.

Figure 11 provided clear evidence that particles moved both up and down at all measuring positions. This caused an extensive turbulence in the gas-solid flow, as indicated in the standard deviation profiles in Figures 6, 7, and 15. From Figures 10 and 11, it can be found that along the radial direction, the downflowing particle velocities have no apparent variation with operating conditions and spatial positions, and most measurements fall into the range of -0.8 to -1.2 m/s. This velocity range was consistent with the mean descending cluster velocities (0.5–2.0 m/s) reported by Bader et al.,[33] Hartge et al.,[34] and Noymer and Glicksman.[35] This suggested that in the high-density gas-solid suspension, the downflowing particles were in a segregated form with a similar falling velocity. Clearly, more experimental work was needed to provide a wider range of data basis, before a more comprehensive explanation can be offered.

Figure 12 showed the time fraction of upflowing particle velocity, $f_{p,up}$, along the radial direction at different operating conditions. $f_{p,up} = N_{p,up}/N_t$, where $N_{p,up}$ was the number of upflowing particle velocities measured during the sampling time, and N_t was the total number of velocity data obtained. For all operating conditions, $f_{p,up}$ was larger than 50% across the entire section but decreased gradually towards the wall. This was understandable given the lower solids concentration in the central region and higher concentration near the wall. Increasing G_s and/or U_g increased $f_{p,up}$, especially in the center region. This statistical analysis indicated that the upward movements of solids dominated the net solids flow direction throughout the whole cross-section of the column.

Figure 13 plotted the time fraction of upflowing particle velocity, $f_{p,up}$, against the corresponding time mean solids concentration, ε_s. The data were collected form all four operating conditions and at all measuring positions. The results gave a good connection between the local solids concentra-

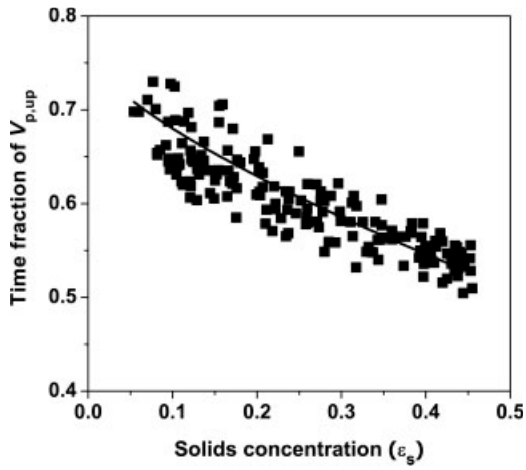

Figure 13. Relationship between the time fraction of upflowing particle velocity and solids concentrations.

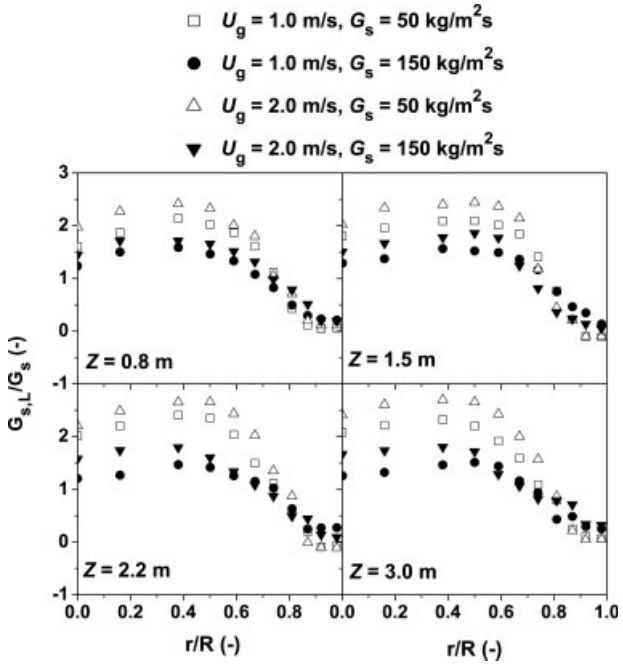

Figure 14. Radial solids flux profile in C-TFB.

tion and the particle velocity. As shown, $f_{p,up}$ decreased monotonously with increasing ε_s. For the same ε_s, f_{pup} was similar, regardless of the operating conditions and spatial positions. The result indicated that at least for the high-density gas-solid flow, there appeared to be a good correlation between the time fraction of particle velocity and the mean solids concentration.

Local solids flux

Radial distribution of reduced solids flux (local solids flux, calculated from the corresponding solids concentrations and velocities, divided by the over mean flux of the entire system) was shown in Figure 14.

Results showed that solids backmixing phenomenon, which was obvious in both turbulent fluidized bed and circulating fluidized bed, was greatly reduced for C-TFB as reflected by the fact that the net time mean flow was always positive at all radial positions, except at the middle axial section (Z = 1.5 and 2.2 m), where negligible downflowing particles were observed at the near wall region at the low solids circulation rates (G_s = 50 kg/m^2 s). And the maximum solids flux occurred somewhere midway between the axis of the column and the wall. This result suggested that high G_s might provide some momentum to support the particles to move upwards and the increased particle concentration resulted in a higher effective viscosity of the rising suspension, thereby imposing more shears on the descending particles.[18] High solids concentration would also increase the inter-particle collision, which could reduce the tendency for the solids downflow. The lack of net solids back-mixing was one of main advantages of the C-TFB, which may lead to a reduction in the extent of axial dispersion of gas carried by the downflowing particles.[36]

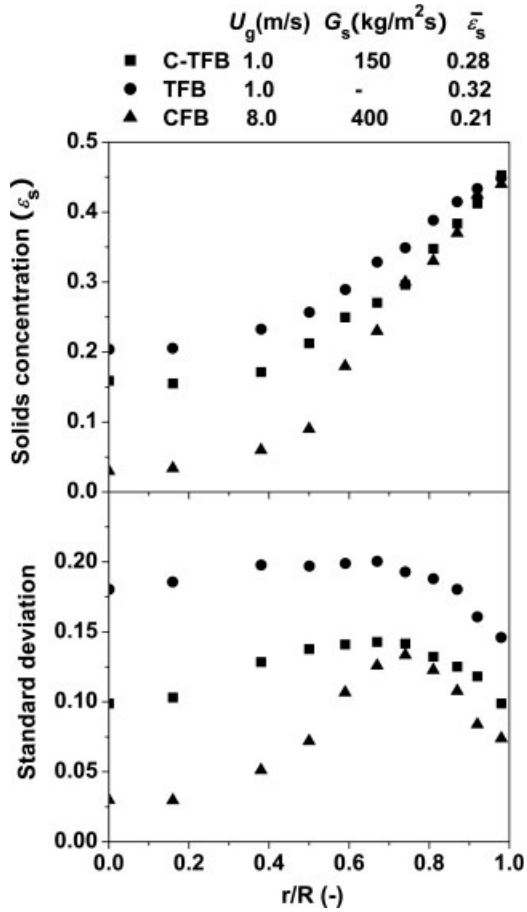

Figure 15. Flow comparison between C-TFB, CFB, and TFB.

Comparison with TFB and bottom dense region of CFB riser

The flow structure comparison between the C-TFB, turbulent fluidized bed (TFB) and the "conventional" or "regular" circulating fluidized bed (CFB) in the viewpoint of radial solids distribution was displayed in Figure 15. Operating conditions in the three fluidization systems were summarized in Table 4.

The comparison showed that the radial solids distribution in the C-TFB became much more uniform than that in the CFB, and closer to that of a conventional TFB. Although there was still an obvious radial gradient in solids concentration distribution in C-TFB, the variation was continuous, rather than exhibiting a sharply demarcated 'core-annulus' flow structure observed in the CFB. Previous studies showed that even in high density and/or high flux CFB risers[17,21] there still existed a definite dilute core region surrounded by dense region adjacent to the riser wall. The low gas velocity

Table 4. Operating Conditions and Geometry

	Geometry (m)	Operating Conditions
C-TFB	i.d. = 0.102, Z = 0.8	U_g = 1 m/s, G_s = 150 kg/m^2 s
TFB	i.d. = 0.102, Z = 0.8	U_g = 1 m/s, G_s = 10 kg/m^2 s
CFB	i.d. = 0.076, Z = 0.8	U_g = 8 m/s, G_s = 400 kg/m^2 s

Table 5. Key Features of Some Fluidized Beds for Group A Particles

	Typical U_g (m/s)	Typical $\bar{\varepsilon}_s$(-)	Key Flow Features
Circulating fluidized beds	>3	~0.03–0.10	• Nonuniform axial flow structure with a dense region at the bottom and a dilute region at the top; • Core-annulus flow structures, with solids movingly mostly downwards at wall.
High density circulating fluidized beds	>6 (refer to Grace[3])	~0.10–0.20	• No net downflow of particles at the wall; • Axial profiles of solids concentration become relatively even; • Considerable radial solids concentration gradient, dilute interior with a denser ring at wall.
Turbulent fluidized beds	~0.5–1.5	~0.25–0.35	• No clear continuous dilute or dense phase, vigorous gas-solid contacting; • Significant gas/solids back-mixing.
Circulating turbulent fluidized beds	~1–3	~0.20–0.30	• Nearly homogenous axial flow structure with high solids concentration maintained through the whole fluidized bed; • No net downflow of solids over the whole fluidized bed; • Smooth increase of solids concentration with radial position with no clear boundary.

and high solids flow rate conditions in the C-TFB greatly reduced the solids radial segregation phenomenon, which was encountered in conventional high velocity CFBs. The solids concentration in C-TFB was very similar to that in TFB, but with the high solids circulation rates in the C-TFB, the fluctuations were lower especially in the central region. This could be interpreted by the fact that the high solids circulation rate greatly reduced the serious solids inner-recycle in TFB, and consequently reduced the fluctuations in solids concentration. Key flow features of fluidized beds including fast fluidized bed, high-density CFB, TFB, and the C-TFB were summarized in Table 5. It was notable that the C-TFB has similarities and differences to both TFB and high density CFB. A more detailed comparison will be provided in a future publication.

General Discussions

CFB have been widely used in various industrial applications. Despite many advantages like high throughput per unit reactor volume and improved gas-solid interaction, the overall gas-solids contacting efficiency and the state of axial and radial gas and solids mixing quality in CFBs were not always optimal. A conceptual novel C-TFB was established to integrate the advantages of both circulating and TFBs. Preliminary investigation in the C-TFB has been conducted to study the overall flow behavior and indicated a promising way to get an attractive new reactor with an ideal environment for rapid heat and mass transfer and good mixing of solids which could lead to a maximum conversion rate per unit volume. Experimental results have revealed that the C-TFB, featured by high solids holdups and high G_s, offered the following more favorable reactor conditions over the conventional circulating and TFBs: (i) recycling of solids, while maintaining a high solids hold-up and intense gas-solids mixing, (ii) no net downflow of solids over the whole section of the C-TFB, (iii) nearly homogenous axial flow structure and enforced homogeneity of suspension in radial direction, and (iv) high degree of operating flexibility. Three factors initiated the C-TFB: (1) pressure differences resulted from the addition of secondary air supply and a quick discharging section with enlarged cross-sectional area; (2) sufficient solids inventory in downcomer to provide pressure head; (3) increased lift forces generated by high-dense upflowing suspension.

Promising application of the C-TFB is fast (but not super fast) reactions involving both gas and solids phases, especially in which a high degree of conversion of the gas phase is required, and the gas-solids contacting efficiency is crucial. Although, current experimental results have given valuable information on this fully high-density flow conditions, it is far away for researcher to develop a theoretical model to describe this new process. Further investigation is required to fully understand the implications of the results and to comprehend the advantages of the C-TFBs. Especially, more work is required to test this system in wider operating conditions and study the effects of other design parameters, such as bed geometry and particle properties, on the hydrodynamic behaviors. It is of importance to detail the dynamic structure of each phase and the dispersion of gas and solids into two phases so as to quantify the actual mass transfer in the C-TFB. Gas and solids phase residence time distribution measurements are also essential.

Optimization of this fluidization system based on detailed mechanisms is necessary before practical applications. Even better performance could be expected from the C-TFB with more optimum mechanical design and operating conditions. The successful development of this new gas-solids fluidized bed also reveals that there is still potential for further development to improve the performance of fluidized bed reactors.

Conclusions

In this article, a novel C-TFB has been presented. The purpose of this new design was to integrate the advantages of both circulating fluidized bed riser and turbulent fluidized bed. Hydrodynamic characteristics of the C-TFB including differential pressure, solids concentration, velocity and flux distribution have been evaluated in a cold-flow set-up with low gas velocity (U_g = 1–2 m/s) and high solids flow rate (G_s = 50–150 kg/m^2 s). The success of the C-TFB was clearly observed from the experimental results. Solids suspension having solids volume concentrations around 0.25–0.30 could be maintained throughout the entire C-TFB. The C-TFB exhibited an almost homogeneous axial flow structure with no net downflow of solids across the whole section

under all operating conditions. Analyses of the probability distribution of solids concentration at all radial positions indicated a better gas-solids contacting than conventional CFB reactors. The solid flow properties in the C-TFB were also compared with that of CFB and TFB, showing that the C-TFB possessed the flow properties of both high-density CFBs and TFBs.

Notation

$f_{p,up}$ = time fraction of upflowing particle velocity
G_s = solids circulation rate measured by butterfly valve, kg/m^2 s
$\overline{G}_{s,L}(t)$ = local time-mean solids flux, kg/m^2 s
G_s^* = calculated solids circulation rate, kg/m^2 s
r = radial distance from column axis, m
R = radius of column, m
U_g = superficial velocity of gas in bed, m/s
$V_{p,up}$ = upflowing particle velocity, m/s
$V_{p,down}$ = downflowing particle velocity, m/s
Z = height above gas distributor, m

Greek letters

ρ_p = particle density, kg/m^3
ε_s = solids volume concentration
$\bar{\varepsilon}_s$ = cross-sectional averaged solids volume concentration
σ = standard deviation

Literature Cited

1. Kunii D, Levenspiel O. *Fluidization Engineering*. London: Butterworth-Heinmann, 1991.
2. Grace JR, Bi HT. Introduction to circulating fluidized beds. In: Grace JR, Avidan AA, Knowlton TM, editors. *Circulating Fluidized Beds*. London: Chapman & Hall,1997:1–18.
3. Grace JR. Reflections on turbulent fluidization and dense suspension upflow. *Powder Technol*. 2000;113:242–248.
4. Li Y, Kwauk M. The dynamics of fast fluidization. In: Grace JR, Matsen JM, editors. *Fluidization*. New York: Plenum Press, 1980: 537–544.
5. Bai DR, Jin Y, Yu ZQ, Zhu JX. The axial distribution of the cross-sectionally averaged voidage in fast fluidized beds. *Powder Technol*. 1992;71:51–58.
6. Issangya AS, Bai D, Bi HT, Lim KS, Zhu J, Grace JR. Suspension densities in a high-density circulating fluidized bed riser. *Chem Eng Sci*. 1999;54:5451–5460.
7. Yerushalmi J, Avidan A. High velocity fluidization. In: Davidson JF, Clift R, Harrison D, editors. *Fluidization*. London: Academic Press, 1985:225–291.
8. Bai D, Shibuya E, Masuda Y, Nishio K, Nakagawa N, Kato K. Distinction between upward and downward flows in circulating fluidized beds. *Powder Technol*. 1995;84:75–81.
9. Nieuwland JJ, Meijer R, Kuipers JAM, van Swaaij WPM. Measurements of solids concentration and axial solids velocity in gas-solid two-phase flows. 1996;87:127–139.
10. Dry RJ, Christensen IN, White CC. Gas-solids contact efficiency in a high-velocity fluidised bed. 1987;52:243–250.
11. Divilio RJ, Boyd TJ. Practical implications of the effect of solids suspension density on heat transfer in large-Scale CFB boilers. In: Avidan AA, editor. *Circulating Fluidized Bed Technology, Vol. IV*. New York: AIChE, 1994:334–339.
12. Lim KS, Zhu JX, Grace JR. Hydrodynamics of gas-solid fluidization. *Int J Multiphase Flow*. 1995;21:141–193.
13. Bi HT, Ellis N, Abba IA, Grace JR. A state-of-the-art review of gas-solid turbulent fluidization. *Chem Eng Sci*. 2000;55:4789–4825.
14. Bi HT, Zhu JX. Static instability analysis of circulating fluidized beds and concept of high-density risers. *AIChE J*. 1993;39:1272–1280.
15. Zhu JX, Bi HT. Distinctions between low density and high density circulating fluidized beds. *Can J Chem Eng*. 1995,73:644–649.
16. Issangya AS, Bai D, Grace JR, Lim KS, Zhu J. Flow behaviour in the riser of high-density circulating fluidized bed. *AIChE Symp Ser*. 1997;93:25–30.
17. Issangya AS, Grace JR, Bai DR, Zhu JX. Further measurements of flow dynamics in a high-density circulating fluidized bed riser. *Powder Technol*. 2000;111:104–113.
18. Grace JR, Issangya AS, Bai DR, Bi HT, Zhu JX. Situating the high-density circulating fluidized bed. *AIChE J*. 1999;45:2108–2116.
19. Kim SW, Kirbas G, Bi HT, Lim CJ, Grace JR. Flow behaviour and regime transition in a high-density circulating fluidized bed riser. *Chem Eng Sci*. 2004:59:3955–3963.
20. Bi XT. Gas and solid mixing in high-density CFB risers. *Int J Chem Reactor Eng*. 2004;2:A12.
21. Pärssinen JH, Zhu JX. Axial and radial solids distribution in a long and high-flux CFB riser. *AIChE J*. 2001;47:2197–2205.
22. Pärssinen JH, Zhu JX. Particle velocity and flow development in a long and high-flux circulating fluidized bed riser. *Chem Eng Sci*. 2001;56:5295–5303.
23. Manyele SV, Pärssinen JH, Zhu JX. Characterizing particle aggregates in a high-density and high-flux CFB riser. *Chem Eng J*. 2002;88:151–161.
24. Mastellone ML, Arena U. The effect of particle size and density on solids distribution along the riser of a circulating fluidized bed. *Chem Eng Sci*. 1999;54:5383–5391.
25. Zhang H, Johnston PM, Zhu JX, de Lasa HI, Bergougnou MA. A novel calibration procedure for a fiber optic solids concentration probe. *Powder Technol*. 1998;100:260–272.
26. Werther J, Hage B, Rudnick C. A comparison of laser Doppler and single-fibre reflection probes for the measurement of the velocity of solids in a gas-solid circulating fluidized bed. *Chem Eng Process*. 1996;35:381–391.
27. Reddy BV, Basu P. Effect of pressure and temperature on cluster and particle heat transfer in a pressurized circulating fluidized bed. *Int J Energy Res*. 2001;25:1263–1274.
28. Louge M, Chang H. Pressure and voidage gradients in vertical gas-solid risers. *Powder Technol*. 1990;60:197–201.
29. Malcus S, Cruz E, Rowe C, Pugsley TS. Radial solid mass flux profiles in a high-suspension density circulating fluidized bed. *Powder Technol*. 2002;125:5–9.
30. Marzocchella A, Zijerveld RC, Schouten JC, van den Bleek CM. Chaotic behavior of gas–solids flow in the riser of a laboratory-scale circulating fluidized bed. *AIChE J*. 1997;43:1458–1468.
31. Cui HP, Mostoufi N, Chaouki J. Characterization of dynamic gas-solid distribution in fluidized beds. *Chem Eng J*. 2000;79:133–143.
32. Bai D, Issangya AS, Grace JR. Characteristics of gas-fluidized beds in different flow regimes. *Ind Eng Chem Res*. 1999;38:803–811.
33. Bader R, Findlay J, Knowlton TM. Gas/solid flow patterns in a 30.5-cm-diameter circulating fluidized bed. In: Basu P, Large JF, editors. *Circulating Fluidized Bed Technology, Vol. II*. Oxford: Pergamon Press,1988:161–165.
34. Hartge EU, Rensner D, Werther J. Solids concentration and velocity patterns in circulating fluidized beds. In: Basu P, Large JF, editors. *Circulating Fluidized Bed Technology, Vol. II*. Oxford: Pergamon Press,1988:165–180.
35. Noymer PD, Glicksman LR. Near-wall hydrodynamics in a scale-model circulating fluidized bed. *Int J Heat Mass Transfer*. 1999; 42:1389–1403.
36. Liu JZ, Grace JR, Bi HT, Morikawa H, Zhu JX. Gas dispersion in fast fluidization and dense suspension upflow. 1999;54:5441–5449.

Manuscript received Jan. 18, 2007, and revision received Dec. 10, 2007.